

# Spin effects in transport through non-Fermi liquid quantum dots

Fabio Cavaliere<sup>1,3</sup> Alessandro Braggio<sup>2</sup>, Maura Sasseti<sup>1</sup>, and Bernhard Kramer<sup>3</sup>

<sup>1</sup>*Dipartimento di Fisica Università di Genova, INFN-LAMIA,  
Via Dodecaneso 33, I-16146 Genova*

<sup>2</sup>*Institut für Theoretische Physik III,  
Universitätsstrasse 150 D-44801 Bochum*

<sup>3</sup>*I. Institut für Theoretische Physik,  
Universität Hamburg, Jungiusstraße 9, D-20355 Hamburg*

(Dated: May 18, 2004)

The current-voltage characteristic of a one dimensional quantum dot connected via tunnel barriers to interacting leads is calculated in the region of sequential tunneling. The spin of the electrons is taken into account. Non-Fermi liquid correlations implying spin-charge separation are assumed to be present in the dot and in the leads. It is found that the energetic distance of the peaks in the linear conductance shows a spin-induced parity effect at zero temperature  $T$ . The temperature dependence of the positions of the peaks depends on the non-Fermi liquid nature of the system. For non-symmetric tunnel barriers negative differential conductances are predicted, which are related to the participation in the transport of collective states in the quantum dot with larger spins. Without spin-charge separation the negative differential conductances do not occur. Taking into account spin relaxation destroys the spin-induced conductance features. The possibility of observing in experiment the predicted effects are briefly discussed.

PACS numbers: 73.63.Kv, 71.10.Pm, 72.25.-b

## I. INTRODUCTION

Spin phenomena in the transport properties of low-dimensional quantum systems have become a subject of increasing interest.<sup>1,2</sup> Several important effects have been found when controlling transport of electrons one by one in quantum dots. For instance, a parity effect in the Coulomb blockade<sup>3</sup> of quantum dots with very small numbers of electrons, and in Carbon nanotubes<sup>4,5</sup> have been detected. The spin blockade effect, especially in the non-linear current-voltage characteristic of one-dimensional (1D) quantum dots has been predicted.<sup>6,7</sup> Combining the spin blockade with spin-polarized detection, the electron spin in a lateral quantum dot has been probed, and spin-related phases were found that have been associated with correlations between the electrons.<sup>8</sup>

The former parity effect is related to the Pauli principle and is quantitatively affected by the contribution of the exchange interaction towards the energy of the ground state of the electrons occupying the quantum dot. The spin blockade effect, which leads to a negative differential conductance (NDC) in the current as a function of the bias voltage, is due to a combined influence of the exchange contribution to the energies of the correlated electronic eigenstates and the spin selection rules for the transport processes. For example, an excited  $n$ -electron state of a quantum dot generally can be depopulated via two spin channels, namely either by increasing or by decreasing the  $z$ -component of the total spin,  $s$ , by  $1/2$ . However, when the state *with the highest total spin* becomes populated at a certain bias voltage  $V$ , it can be depopulated only via processes that decrease  $s$ . This can lead to a reduction of the total current  $I(V)$ , when in-

creasing the bias voltage, thus yielding  $\partial I/\partial V < 0$ .

This phenomenon has been predicted by using a simple model for the transport mediated by sequential electron tunneling processes through a 1D quantum dot containing few electrons ( $n \leq 4$ ). The electronic eigenstates of the latter have been determined numerically exactly in the presence of interactions and spin.<sup>6,7</sup> The tunneling matrix elements of the barriers connecting the states of the quantum dot to those in the Fermi-liquid leads were assumed to include spin selection rules via Clebsch-Gordan coefficients and assuming *ad hoc* some tunneling coupling matrix elements between the correlated quantum dot states and the states in the leads. Only later, the matrix elements have been calculated microscopically in order to test the former assumptions.<sup>9</sup> There are several, in the details somewhat different and intricate mechanisms that produce such a spin-induced reduction of the current. Characteristic dependences on the magnetic field may be used to distinguish between them. While certain signatures of these features have been found in a recent experiment done on 2D quantum dot,<sup>10</sup> experimentally well-controlled evidence in quasi-1D quantum dots is missing.

The recent experimental realization of semiconductor-based 1D quantum wires<sup>11,12,13</sup> has opened new perspectives to systematically investigating the influence of interactions, spins and impurities on electron transport properties. Signatures of spin-charge separation have been observed<sup>14</sup> and analyzed<sup>15</sup> in the tunneling between parallel one-dimensional wires. Also carbon nanotubes can now be controlled to such a high degree that investigations of electronic transport features have become possible.<sup>4,5,16,17</sup> The effects of non-Fermi liquid correla-

tions in 1D quantum dots have been analyzed non perturbatively in the *coherent* tunneling regime.<sup>18,19</sup>

In the non-linear transport spectra of these devices, obtained as the derivative of the current-voltage characteristics at different gate voltages, a large number of low-energy excited states have been found.<sup>20</sup> These cannot be understood only in terms of charge excitations<sup>21</sup> but are theoretically predicted to be related also to the spin.<sup>22</sup> Thus, one can expect that 1D spin blockade effects could be seen in an experiment. Among the experimental realizations of 1D quantum dots are electron islands between two successive impurities in a 1D quantum wire (containing interacting electrons) and carbon nanotubes. Thus an extension to the theory of the blockade effects should include not only the generalization to higher electron densities—the previous calculations have been done in the limit of low electron density—but treat the interactions and the spins within the quantum dot and within the leads on an equal footing.

There are perspectives for application of quantum structures in spin-electronics, quantum computing and communication.<sup>23</sup> Previous works focused on spin transport in (2D) quantum dots connected to non-interacting leads in the presence of a magnetic field,<sup>24</sup> including an oscillating magnetic electron spin resonance component.<sup>25</sup> Spin transport in circuits with ferromagnetic elements and Luttinger-liquid interaction<sup>26,27,28</sup> has been considered. In view of the applications, the theory of the spin control of electron transport in the presence of correlations is very important since in nanoscale devices the latter can be very important. In our previous work,<sup>22</sup> we have found that at  $T = 0$ , spin polarization effects are robust against the correlations. They can even be enhanced, if the polarization is not complete.

In the present paper, we extend our previous calculations to include temperature effects, asymmetry in the tunnel barriers and the effect of spin relaxation. The former are treated microscopically within the sequential tunneling approximation using the microscopic model of a 1D quantum dot described by a Luttinger liquid of finite length connected via tunnel barriers to semi-infinite interacting leads. Spin relaxation is treated phenomenologically by including tunnel rates corresponding to spin-flip transitions into the master equation for the dynamics of the probability distribution. Our main results are

1. We deduce that the temperature dependence of the linear conductance peaks reflects the non-Fermi liquid correlation in the leads.
2. In non-linear transport, we find that many-particle states with higher spins in the quantum dot act as traps such that the electric current decreases with increasing bias voltage. The physical origin of this is spin-charge separation.
3. Spin relaxation leads to a destruction of the negative differential conductance peaks. This confirms that they are related to the trap properties

of higher-spin states. A typical “phase diagram” of the crossovers between negative and positive differential conductance peaks is calculated.

We discuss the quantitative conditions for observing the predicted effects in an experiment.

In the next section, we introduce the model for the Luttinger liquid quantum dot. Section 3 is used to discuss the energy scales of the system. In the section 4 we describe the approach for calculating the transport properties. Section 5 is devoted to the linear and section 6 to the non-linear regime. In section 7 we compare with other recent approaches, discuss possible experimental realizations and draw some conclusions.

## II. TOMONAGA-LUTTINGER MODEL FOR A 1D QUANTUM DOT WITH SPIN

We consider the 1D system shown schematically in Fig. 1. The region  $|x| < a/2$  represents a finite quantum wire that plays the role of the 1D quantum dot. This is assumed to be connected to reservoirs with electrochemical potentials  $\mu_\lambda = \pm eV/2$  ( $\lambda = R, L$ ) via semi-infinite 1D systems between  $-L < x < -a/2$  and  $a/2 < x < L$  ( $L \rightarrow \infty$ ) that represent left (L) and right (R) leads, respectively. The electrochemical potentials are controlled by the bias voltage  $V$ . Tunneling barriers at  $x = \pm a/2$  connect the quantum dot with the leads. The three

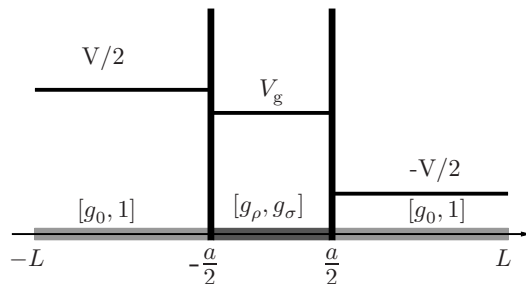


FIG. 1: Schematic representation of the Luttinger liquid quantum dot ( $|x| < a/2$ ) connected via tunneling barriers to semi-infinite wires. The charge ( $g_\rho$ ) and spin ( $g_\sigma$ ) interaction parameters in the leads and the dot are assumed to be different. The bias voltage  $V$  controls the chemical potential difference of the leads. The gate voltage  $V_g$  controls the chemical potential quantum dot (cf. Fig. 2).

regions of the quantum wire are assumed as interacting Luttinger liquids (LL)<sup>29,30,31,32</sup> with possibly *different* interaction constants for charges ( $g_\rho$ ) and spins ( $g_\sigma$ ) (Fig. 1).<sup>33,34</sup> In addition to the bias voltage  $V$  we assume that the chemical potential in the dot region is tuned via a gate voltage  $V_g$ . The total Hamiltonian is

$$H = H_0 + H_t + H_c. \quad (1)$$

Here,  $H_0 = H_0^{(d)} + H_0^{(L)} + H_0^{(R)}$  describes the three uncoupled LL,  $H_t$  the tunneling term, and  $H_c$  the coupling with the external electric circuit.

The 1D quantum dot ( $|x| < a/2$ ) is treated with open boundary conditions,<sup>35,36</sup>  $\psi_s^{(d)}(\pm a/2) = 0$ , with the fermion operators  $\psi_s^{(d)}(x)$  corresponding to the  $z$ -component of the spin  $s = \pm 1$  (unit  $\hbar/2$ ).

The Luttinger liquid theory describes the energetically low-lying excitations of 1D interacting electrons around the Fermi energy  $E_F$ . It relies on the linearization of the dispersion relation around the Fermi level giving rise to a bare, constant level spacing  $\varepsilon_0 = \hbar\pi v_F/a$ . As a necessary condition for this assumption, one needs to fulfill the condition  $E_F \gg \varepsilon_0$ . For a system of finite length, this implies a constraint between the Fermi wave number and the momentum discretization,  $k_F \gg \pi/a$ . There is also a constraint with respect to temperature induced by the finite size of the dot. In order to resolve the energy levels of the correlated states the temperature should be lower than the level spacing,  $k_B T \ll \varepsilon_0$ .

Near the Fermi point  $k_F$  the fermion operators are decomposed into fields that propagate to the right (r) and to the left (l)

$$\psi_s^{(d)}(x) = e^{ik_F x} \psi_{s,r}^{(d)}(x) + e^{-ik_F x} \psi_{s,l}^{(d)}(x). \quad (2)$$

Because of the boundary conditions these fields are not independent. The bosonization description is done using only  $\psi_{s,r}^{(d)}(x)$ . The system is diagonalized in the presence of interactions. The corresponding Hamiltonian is<sup>35,36</sup> (units such that  $\hbar = 1$ )

$$H_0^{(d)} = \sum_{\nu=\rho,\sigma} \sum_{q>0} \omega_\nu(q) \nu^\dagger(q) \nu(q) + \frac{\pi}{4a} \left[ \frac{v_\rho}{g_\rho} \hat{n}^2 + \frac{v_\sigma}{g_\sigma} \hat{s}^2 \right]. \quad (3)$$

Here,  $\nu^\dagger(q)$ ,  $\nu(q)$  are the boson operators of the collective charge ( $\nu = \rho$ ) and spin ( $\nu = \sigma$ ) density waves (CDW and SDW). Due to the boundary condition the wave number is quantized,  $q = \pi m/a$  ( $m$  integer  $\geq 1$ ). The energy spectra are<sup>29</sup>

$$\omega_\nu(q) = v_\nu q, \quad v_\nu = \frac{v_F}{g_\nu} (1 + V_{\text{ex}}) \quad (4)$$

with the interaction parameters

$$g_\rho^2 = \frac{1 + V_{\text{ex}}}{1 - V_{\text{ex}} + 4V_0}, \quad g_\sigma^2 = \frac{1 + V_{\text{ex}}}{1 - V_{\text{ex}}} \quad (5)$$

where

$$V_0 = \frac{\hat{V}(0)}{2\pi v_F}, \quad V_{\text{ex}} = \frac{\hat{V}(2k_F)}{2\pi v_F} \quad (6)$$

are proportional to the forward ( $q \rightarrow 0$ ), and part of the backward ( $q \rightarrow 2k_F$ ) contributions of the electron interaction, respectively. The quantity  $\hat{V}(q)$  denotes the Fourier transform of the interaction potential inside the dot. The backward term corresponds to an exchange interaction. The parameters fulfill  $V_{\text{ex}} < 1$ , necessary in order to have a bounded Hamiltonian, and  $V_0 > V_{\text{ex}}$ . This implies  $0 < g_\rho \leq 1$  (repulsive charge-charge interaction) and  $g_\sigma \geq 1$ .

The zero mode operators  $\hat{n}$  and  $\hat{s}$  represent the excess number of charges, and of the  $z$ -component of the total spin with respect to their average values on the ground state. The latter correspond to  $n_0 = 2k_F a/\pi - 1$  and  $s_0 = 0$  in the absence of a magnetic field. The eigenvalues of the zero-mode operators are integers  $n, s$  with the constraint, due to the boundary conditions,  $n + s = \text{even}$ . The zero-mode energy contributions in (3) represent the energy needed for changing the total charge and spin with respect to the ground state.

For the leads we assume a LL with open boundary conditions at the tunnel barriers. At  $L = \pm\infty$  they are assumed to be connected to reservoirs with different electrochemical potentials. The difference of the latter is proportional to the bias voltage. In state-of-the-art semiconductor quantum wires (and also in carbon nanotube systems) the exchange is only a very small correction as compared to the Coulomb part of the interaction<sup>37</sup> which in any case is expected to be considerably weaker than in the region of the quantum dot. The exchange interaction in the leads is not expected to influence the results described below on the qualitative level. Especially, it is not expected to influence the positions of the conductance peaks that are determined by the interactions in the region of the quantum dot. At most, it can give a small quantitative correction of the dependence on temperature of the conductance peaks which is determined by the global properties of the system as has been discussed earlier.<sup>34</sup> Therefore, we neglect in this paper the exchange interaction in the leads completely for the sake of simplicity. The Hamiltonian describing the excitations in the leads is then<sup>29</sup>

$$H_0^{(\lambda)} = \sum_{\nu=\rho,\sigma} \sum_{k>0} \Omega_\nu(k) \nu_\lambda^\dagger(k) \nu_\lambda(k) + \frac{\pi \bar{v}_F}{4L} \left[ \frac{1}{g_0^2} \hat{n}_\lambda^2 + \hat{s}_\lambda^2 \right],$$

with  $\bar{v}_F$  the Fermi velocity in the leads,  $\nu_\lambda^\dagger(k)$ ,  $\nu_\lambda(k)$ , the boson operators of collective CDW, SDW and  $\hat{n}_\lambda$ ,  $\hat{s}_\lambda$  the zero mode operators for the excess of charge and spin with respect to their average values in the leads. The energy spectra are ( $k = \pi m/L$ ,  $m$  integer  $\geq 1$ )

$$\Omega_\rho(k) = \frac{\bar{v}_F}{g_0} k, \quad \Omega_\sigma(k) = \bar{v}_F k$$

with the charge interaction parameter  $g_0$

$$g_0 = \left( 1 + \frac{2U_0}{\pi \bar{v}_F} \right)^{-1/2} < 1$$

determined by the average interaction  $U_0$  in the leads.

The coupling between the leads and the dot is described by tunnel barriers at  $x_L = -a/2$  and  $x_R = a/2$

$$H_t = \sum_{s=\pm 1} \sum_{\lambda=L,R} \left[ t_\lambda \psi_{s,r}^{(\lambda)\dagger}(x_\lambda) \psi_{s,r}^{(d)}(x_\lambda) + \text{h.c.} \right], \quad (7)$$

with the right moving fermion operators normalized to the shortest wavelength, and  $t_{L,R}$  the transmission amplitudes of the barriers.<sup>35</sup>

The operator of the external bias and gate voltages that allows to electrically control current transport and charge density in the dot are written in terms of the operators  $\hat{n}$  of the excess charges (Fig. 2)<sup>38</sup>

$$H_c = \frac{eV}{2} [\hat{n}_R - \hat{n}_L] - e \left[ \frac{\delta C}{2C_\Sigma} V + \frac{C_g}{C_\Sigma} V_g \right] \hat{n}. \quad (8)$$

Here,  $V$  and  $V_g$  are the bias and the gate voltage,  $C_\Sigma = C_L + C_R + C_g$  is the total capacitance with  $C_L, C_R$  and  $C_g$  the capacitances of the leads and the gate, where  $\delta C = C_L - C_R$ .

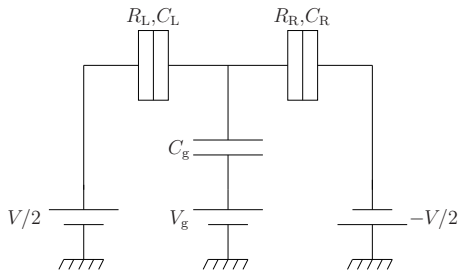


FIG. 2: Equivalent circuit for the quantum dot with asymmetric tunnel barriers. Left and right tunnel junctions are parameterized by the capacitances  $C_{L,R}$  and the resistances  $R_{L,R} \equiv \omega_c^2 / \pi e^2 t_{L,R}^2$  (cf. (25)),  $\omega_c$  cutoff energy of the leads,  $t_{L,R}$  transmission amplitudes of the barriers,  $C_g$  gate capacitance,  $V_g$  gate voltage,  $V$  bias voltage.

### III. ENERGY SCALES

The states of the isolated quantum dot are  $|n, s, \{l_q^\rho\}, \{l_q^\sigma\}\rangle$  where  $n$  and  $s$  are the excess numbers of charges and spins with respect to the ground state with charge  $n_0$  and spin  $s_0$ , and  $\{l_q^\nu\}$  the occupation numbers of the CDW ( $\nu = \rho$ ) and SDW ( $\nu = \sigma$ ) at different  $q$ . Some examples of these states are schematically shown in Fig. 3. Figure 3a represents the state  $|1, 1, \{0\}, \{0\}\rangle$ , corresponding to one excess charge  $n = 1$  with spin  $s = 1$ . Figure 3b shows the state  $|2, 0, \{0\}, \{0\}\rangle$  with two extra electrons and  $s = 0$ . A higher spin state ( $s = 2$ ) is shown in Fig. 3c. Excited states with unchanged  $n$  and  $s$  contain CDW and/or SDW. Figure 3d shows an example with the smallest possible wave-number  $q_0 = \pi/a$  and smallest excitation energy for  $n = 2$  and  $s = 0$ . The operator

$$\sigma^\dagger(q_0) |2, 0, \{0\}, \{0\}\rangle = |2, 0, \{0 \dots\}, \{1, 0, \dots, 0, \dots\}\rangle.$$

creates a linear superposition of the state (cf. Fig. (3d)) and the one with inverted spins. In the presence of interaction a charge excitation with the smallest wave number would be associated with a much larger excitation energy.

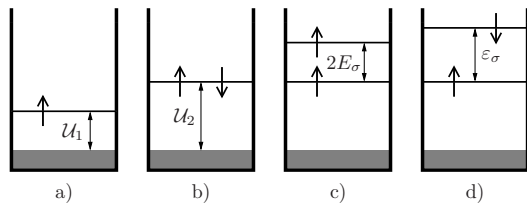


FIG. 3: Schematic examples of excited states with respect to a background charge  $n_0 = (2ak_F/\pi) - 1$  and spin  $s_0 = 0$ . (a)  $n = 1$  and  $s = 1$ ,  $\mathcal{U}_1 \equiv \mathcal{U}(1, 1, 0, 0)$  (see Eq. (9)), (b)  $n = 2$  and  $s = 0$ ,  $\mathcal{U}_2 \equiv \mathcal{U}(2, 0, 0, 0)$ , (c) excited state with  $s = 2$  for  $n = 2$ , (d) spin excitation with respect to the state (b).

Excitations with higher wave numbers induced by operators  $\nu^\dagger(q > q_0)$ , as well as multiple excitations  $[\nu^\dagger(q)]^r$  ( $r > 1$ ) are also possible.

Using the Hamiltonian (3) we write the total energy of the particular configuration  $|n, s, \{l_q^\rho\}, \{l_q^\sigma\}\rangle$  as

$$\mathcal{U}(n, s, l_\rho, l_\sigma) = \frac{E_\rho}{2} n^2 + \frac{E_\sigma}{2} s^2 + l_\rho \varepsilon_\rho + l_\sigma \varepsilon_\sigma. \quad (9)$$

The first two terms represent the contributions of charge and spin additions. The second two terms correspond to the CDW and SDW. Since the excitation spectra are linear in the wave number, the energies of the collective modes depend on the total numbers of excitation quanta  $l_\nu = \sum_q q l_q^\nu$  only via the discrete excitation energies  $\varepsilon_\nu = \pi v_\nu / a$ . From the microscopic theory one gets ( $\nu = \rho, \sigma$ )

$$E_\nu = \frac{\pi v_\nu}{2ag_\nu} = \frac{\varepsilon_0}{2} \frac{1 + V_{\text{ex}}}{g_\nu^2}, \quad (10)$$

where  $\varepsilon_0 = \pi v_F / a$  the constant level spacing in the non-interacting case. These energies are different from zero even without interaction due to the discrete nature of the energy levels inside the dot and the Pauli principle.

Despite the microscopic model provides quantitative estimates for the charge and spin addition energies, several influences that occur in experimental setups are here neglected. For instance, the coupling with the gates, long range interaction effects, and the screening due to the nearby 2DEG present in cleaved edge overgrowth systems<sup>13,20</sup> affect  $E_\rho$  and can cause strong deviations from the simple expression (10).<sup>21</sup> More robust is the spin addition energy which is influenced at most by the exchange part of the interaction. Therefore, we treat in the following  $E_\rho$  as a free parameter with  $E_\rho \gg E_\sigma$ .

Phenomenologically, one identifies  $E_\rho$  with the total electrostatic energy (Fig. 2)  $E_\rho = e^2 / C_\Sigma$  of the circuit model. With this one includes the term  $enV_g C_g / C_\Sigma$  coming from (8) into the zero mode of the charge sector in (9),  $E_\rho (n - n_g)^2 / 2$  with  $n_g = V_g C_g / e$ .

For the spin addition energy we continue using the microscopic expression (10)

$$E_\sigma = \frac{\varepsilon_0}{2} (1 - V_{\text{ex}}).$$

Due to the exchange interaction this energy is decreased as compared to the non-interacting case. The energy quanta of the collective excitations can be expressed microscopically as

$$\varepsilon_\nu = \varepsilon_0 \frac{1 + V_{\text{ex}}}{g_\nu}. \quad (11)$$

The presence of the exchange interaction renormalizes simultaneously the energy  $E_\sigma$  of the total spin configuration and the energy  $\varepsilon_\sigma$  of the spin waves

$$\varepsilon_\sigma = \varepsilon_0 \sqrt{1 - V_{\text{ex}}^2} = 2E_\sigma \sqrt{\frac{1 + V_{\text{ex}}}{1 - V_{\text{ex}}}}$$

The plasmon energy  $\varepsilon_\rho$  is, on the other hand, affected by the Coulomb interaction with in general  $\varepsilon_\rho > \varepsilon_\sigma$ . The energetic difference between the CDW and SDW indicates the presence of the spin-charge separation in a LL.

The above discussion implies a hierarchy of energy scales characteristic for the model considered

$$2E_\sigma < \varepsilon_\sigma < \varepsilon_0 < \varepsilon_\rho < E_\rho.$$

This suggests to use  $E_\sigma$  as the natural energy scale. Without interaction  $2E_\sigma = \varepsilon_\sigma = \varepsilon_\rho = \varepsilon_0$ .

## IV. TUNNELING

### A. Transition rates

For high tunnel barriers and not too low temperatures, the dominant processes that contribute to the electron transport are sequential transfers of single electrons with spin up or down through the two barriers. In this case,  $H_t$  is treated as a perturbation. Higher order coherent processes can be safely neglected as long as  $k_B T \gg \delta E$ , with  $\delta E$  the level broadening of virtual states proportional to the tunneling rates.<sup>39</sup> We consider processes that change the state of the dot from an initial  $|i\rangle$  to a final state  $|f\rangle$ ,

$$|i\rangle = |n_i, s_i, \{l_{qi}^\rho\}, \{l_{qi}^\sigma\}\rangle, \quad |f\rangle = |n_f, s_f, \{l_{qf}^\rho\}, \{l_{qf}^\sigma\}\rangle.$$

Because of the sequential nature of the tunnel processes these states have to be consistent with the charge and spin selection rules

$$\Delta n \equiv n_f - n_i = \pm 1, \quad \Delta s \equiv s_f - s_i = \pm 1. \quad (12)$$

For obtaining explicitly the tunneling rates  $\Gamma_{|i\rangle \rightarrow |f\rangle}^{(\lambda)}$  across the left ( $\lambda = L$ ) and right barriers ( $\lambda = R$ ) we sum over all possible final lead states and perform a thermal average over the initial states with the chemical potentials  $\mu_\lambda$ . From (7) one finds

$$\Gamma_{|i\rangle \rightarrow |f\rangle}^{(\lambda)} = t_\lambda^2 \varphi_d^\lambda \int_{-\infty}^{\infty} d\tau e^{i\Delta U \tau} e^{-W_i(\tau)}. \quad (13)$$

The matrix element  $\varphi_d^\lambda$  is

$$\varphi_d^\lambda = \left| \langle i | \psi_{s,r}^{(d)}(x_\lambda, 0) | f \rangle \right|^2. \quad (14)$$

The energy difference

$$\Delta \mathcal{U} = \mathcal{U}(|f\rangle) - \mathcal{U}(|i\rangle) - \Delta n \left[ \frac{\delta C}{C_\Sigma} \mp 1 \right] \frac{eV}{2} \quad (15)$$

is obtained from  $\mathcal{U}$  defined in (9). The signs  $\pm$  refer to the left (+) or right (-) barriers, the factor  $\exp[-W_i(t)]$  results from the trace over the lead excitations,<sup>39</sup>

$$e^{-W_i(\tau)} = \left\langle \psi_{s,r}^{(\lambda)\dagger}(x_\lambda, \tau) \psi_{s,r}^{(\lambda)}(x_\lambda, 0) \right\rangle_{\text{leads}}. \quad (16)$$

The thermal average is performed with respect to the decoupled Hamiltonians  $H_0^{(\lambda)}$ . This factor turns out to be independent of the spin of the tunneling electron and the barrier variables. The contribution of the quantum dot is contained in  $\Delta \mathcal{U}$  and in the matrix elements  $\varphi_d^\lambda$ .

The tunneling rates  $\Gamma_{|i\rangle \rightarrow |f\rangle}^{(\lambda)}$  were recently used by Kim *et al.*<sup>40</sup> in order to study the out-of-equilibrium dynamics in the presence of an external voltage. In this work it has been assumed that the collective modes are stable and do not relax during the tunneling processes. The probability distribution was obtained self-consistently using a generalized master equation.

The opposite situation has been addressed by Braggio *et al.*<sup>22</sup> who considered the possibility of fast relaxation of the collective modes induced by extra processes<sup>41</sup> that are not included in the diagonal Hamiltonians  $H_0^{(d)}$ , such as spin-orbit interaction and phonon coupling. In this case, the dynamical variables consist of the total charge and spin only, while the collective modes are traced out with a thermal average over the initial states and a summation over the final states. In the following, we use this second model.

As already pointed out<sup>40</sup>, the two approaches do not give qualitatively different results regarding the current-voltage characteristic of the system. However, in a very recent work,<sup>42</sup> the presence of stable plasmons in a spinless 1D quantum dot has been shown to affect dramatically its shot noise properties. On the contrary it was also predicted a crossover towards the results of a model with fully relaxed bosonic modes<sup>43</sup>, in the presence of a phenomenological relaxation rate for the plasmons. In particular the two models give the same results if  $\gamma_p/\tilde{\Gamma}_0 \gtrsim 1$ , where  $\gamma_p$  is a phenomenological relaxation rate of the plasmonic modes and  $\tilde{\Gamma}_0^{-1} = \Gamma_0^{(L)-1} + \Gamma_0^{(R)-1}$  with  $g_\rho = g_\sigma = 1$  - see Eq. 26 - is a characteristic tunneling rate. In a system with spin, we can expect a similar result if the phenomenological relaxation rate of the spin density waves  $\gamma_s$ , satisfies  $\gamma_s/\tilde{\Gamma}_0 \gtrsim 1$ . For semiconductor-based 1D quantum dots<sup>20</sup> one can estimate  $\tilde{\Gamma}_0 \approx 10^{11} \text{ s}^{-1}$  by using a tunnel resistance  $R_R \approx 100 \text{ h}/e^2$  and  $a \approx 0.2 \text{ }\mu\text{m}$  - see section VII. . It is difficult to evaluate microscopically the relaxation rates  $\gamma_{p,s}$ . However, one

can estimate,<sup>41</sup> using a level spacing of about 1 meV,  $\gamma_s \approx 8 \cdot 10^{12} \text{ s}^{-1}$ . It can be expected that  $\gamma_p$  is even larger. In the following we assume  $\gamma_{p,s}/\tilde{\Gamma}_0 > 1$  and thus complete relaxation of the bosonic modes.

The reduced rates are then given by

$$\Gamma_{|n_i, s_i\rangle \rightarrow |n_f, s_f\rangle}^{(\lambda)} = \sum_{\{l_{qi}^\nu\}} P(\{l_{qi}^\nu\}) \sum_{\{l_{qf}^\nu\}} \Gamma_{|i\rangle \rightarrow |f\rangle}^{(\lambda)} \quad (17)$$

with  $P(\{l_{qi}^\nu\})$  the thermal probability distribution with respect to  $H_0^{(d)}$ . Performing the sums one finds

$$\Gamma_{|n_i, s_i\rangle \rightarrow |n_f, s_f\rangle}^{(\lambda)} = t_\lambda^2 \int_{-\infty}^{\infty} d\tau e^{i\Delta U \tau} e^{-W_1(\tau)} e^{-W_d(\tau)} \quad (18)$$

where

$$\begin{aligned} \Delta U &= \frac{E_\rho}{2} [1 + 2(n_i - n_g) \Delta n] + \frac{E_\sigma}{2} [1 + 2s_i \Delta s] \\ &\quad - \Delta n \left[ \frac{\delta C}{C_\Sigma} \mp 1 \right] \frac{eV}{2} \end{aligned} \quad (19)$$

is the energy difference associated to the particular process, the signs  $\pm$  refers to the left (+) or right (−) barriers. The kernel  $e^{-W_d(\tau)}$  represents the thermal average over the initial spin and charge collective modes in the dot. Using the bosonization method one obtains<sup>35</sup> ( $\beta^{-1} = k_B T$ )

$$\begin{aligned} W_{1,d}(\tau) &= \int d\omega \frac{J_{1,d}(\omega)}{\omega^2} \left\{ \coth\left(\frac{\beta\omega}{2}\right) [1 - \cos(\omega\tau)] \right. \\ &\quad \left. + i \sin(\omega\tau) \right\}. \end{aligned} \quad (20)$$

Here, the spectral densities of the leads and the quantum dot are,

$$J_1(\omega) = \frac{\omega}{g} e^{-\omega/\omega_c} \quad (21)$$

and

$$J_d(\omega) = \omega \sum_{\nu \in \{\rho, \sigma\}} \frac{\epsilon_\nu}{2g_\nu} \sum_{m=1}^{\infty} \delta(\omega - m\epsilon_\nu) e^{-\omega/\omega_c}. \quad (22)$$

The cutoff  $\omega_c$  defines the highest energy in the model and  $g^{-1} = (1 + g_0^{-1})/2$ .

The structure of the spectral density of the dot,  $J_d(\omega)$ , indicates that, though they are infinitely quickly relaxing, the CDW and the SDW still contribute to the tunneling dynamics. Even if the relaxation prevents the collective excitations to be initial states for the tunneling, it is still possible to reach an excited state as a “final” state with a given energy. A typical process is

$$|n_i, s_i\rangle \rightarrow |n_f, s_f, \{l_{qi}^\rho\}, \{l_{qf}^\sigma\}\rangle \Rightarrow |n_f, s_f\rangle \quad (23)$$

where the rightmost process ( $\Rightarrow$  arrow) is associated with a fast time scale and the intermediate state contains collective excitations. In this approximation, only the energy of the collective excitation is detectable. In the following we will use the notation

$$|n, s, l_\rho, l_\sigma\rangle \quad (24)$$

to label an excited state when it is involved as a final state in a tunneling process.

Let us now investigate in more detail the energy dependence of the rates. For simplicity, we do not specify the initial and final spin and charge states. Exploiting the discrete nature of the dot spectral density we rewrite (18) as a function of the energy difference  $E = \Delta U$

$$\Gamma^{(\lambda)}(E) = \Gamma_0^{(\lambda)} \sum_{l_\rho, l_\sigma} a_{l_\rho} a_{l_\sigma} \gamma(E - l_\rho \epsilon_\rho - l_\sigma \epsilon_\sigma), \quad (25)$$

where

$$\Gamma_0^{(\lambda)} = \left(\frac{\epsilon_\rho}{\omega_c}\right)^{1/2g_\rho} \left(\frac{\epsilon_\sigma}{\omega_c}\right)^{1/2g_\sigma} \frac{2\omega_c G_\lambda}{e^2 \Gamma(1 + \alpha)}, \quad (26)$$

with

$$\alpha = \frac{1}{g} - 1 \quad (27)$$

and  $G_\lambda = R_\lambda^{-1} = \pi e^2 t_\lambda^2 / \omega_c^2$  the intrinsic conductances of the barriers. The function  $\gamma(x)$  is determined by the leads<sup>22</sup>

$$\gamma(x) = \frac{1}{2\pi} e^{\beta x/2} \left| \Gamma\left(\frac{1}{2g} + i\frac{\beta x}{2\pi}\right) \right|^2 \left(\frac{2\pi}{\beta\omega_c}\right)^\alpha. \quad (28)$$

At  $T = 0$  we have

$$\gamma^0(x) = \left(\frac{x}{\omega_c}\right)^\alpha \theta(x). \quad (29)$$

The weights  $a_{l_\nu}$  are due to the dot contribution. At  $T = 0$ , they are

$$a_{l_\nu}^0 = \frac{\Gamma(1/2g_\nu + l_\nu)}{\Gamma(1/2g_\nu) l_\nu!} \theta(l_\nu). \quad (30)$$

For finite temperature, the weights have to be numerically determined. In (28)-(30),  $\Gamma(z)$  is the Euler-gamma function. Figure 4 shows the effect of the charge-spin separation in the structure of  $\Gamma^{(\lambda)}(E)/\Gamma_0^{(\lambda)}$  at  $T = 0$ . In the absence of spin-charge separation ( $g_\rho = g_\sigma = 1$ ) all of the energies are degenerate,  $\epsilon_\rho = \epsilon_\sigma = \epsilon_0$ . It is then easy to write down explicitly the contributions to the sum (25)

$$\begin{aligned} &a_0^2 \theta(x) + 2a_0 a_1 \theta(x - \epsilon_0) + (a_1^2 + 2a_0 a_2) \theta(x - 2\epsilon_0) \\ &\quad + 2(a_0 a_3 + a_1 a_2) \theta(x - 3\epsilon_0) + \dots \end{aligned}$$

with  $a_0 = 1$ ,  $a_1 = 1/2$ ,  $a_2 = 3/8$ ,  $a_3 = 5/16$ ,  $\dots$ . Each of the coefficients of the theta-functions in the latter expression sums up to one (Fig. 4), so one always has unit

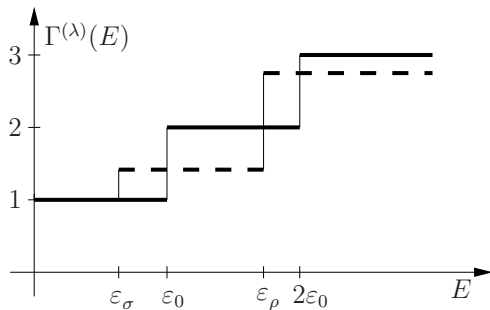


FIG. 4: Schematic plot of the transition rate  $\Gamma^{(\lambda)}(E)$ , in units of  $\Gamma_0^{(\lambda)}$ , as a function of the tunneling energy  $E$ , for  $g_0 = 1$  and  $T = 0$ . Full line: no interactions in the dot,  $g_\rho = g_\sigma = 1$ ; dashed line: with interactions,  $g_\sigma > 1$  and  $g_\rho < 1$ . Excitation energies are indicated at the energy-axis.

steps centered at integer values of  $\varepsilon_0$ . If  $g_\sigma > 1$  and  $g_\rho < 1$ , charge and spin modes are energetically split,  $\varepsilon_\sigma < \varepsilon_0 < \varepsilon_\rho$ . Then, the first three terms of (25) are

$$\theta(x) + \frac{1}{2g_\sigma}\theta(x - \varepsilon_\sigma) + \frac{1}{2g_\rho}\theta(x - \varepsilon_\rho).$$

This implies non-integer quantized steps at different energies with heights depending on the spin and charge interactions (Fig. 4, dashed line). For simplicity, in Fig. 4  $T = 0$  and  $g_0 = 1$  have been assumed. Finite temperatures and  $g_0 < 1$  do not drastically change these results but smoothen the jumps at the positions given by the dot parameters.

## B. The master equation

Having assumed fast relaxation of the collective excitations in the quantum dot necessarily implies that the stationary states of the dot are fully characterized by the variables  $n$  and  $s$ . One can then define an occupation probability  $P(n, s)$  for a state  $|n, s\rangle$  that satisfies the master equation

$$\partial_t P_{n,s}(t) = \sum_{\substack{n'=n\pm 1 \\ s'=s\pm 1}} [P_{n',s'}(t)\Gamma_{|n',s'\rangle\rightarrow|n,s\rangle} - P_{n,s}(t)\Gamma_{|n,s\rangle\rightarrow|n',s'\rangle}], \quad (31)$$

where  $\Gamma \equiv \sum_\lambda \Gamma^{(\lambda)}$ . In the stationary limit, the l.h.s. of (31) is zero such that one has to solve a homogeneous system of linear equations. The solution must be normalized,  $\sum_{n,s} P_{n,s} = 1$ . The stationary current is

$$I = e \sum_{n,s} \sum_{q=\pm 1} P_{n,s} \left[ \Gamma_{|n,s\rangle\rightarrow|n+1,s+q\rangle}^{(R)} - \Gamma_{|n,s\rangle\rightarrow|n-1,s+q\rangle}^{(R)} \right]. \quad (32)$$

If both  $eV, k_B T < E_\rho$  at most two charge states enter the dynamics, and the current is given by tunneling

events corresponding to transitions  $|n, s\rangle \rightarrow |n+1, s'\rangle \rightarrow |n, s''\rangle$ . Below, we will consider this regime.

In the above discussion, it is assumed that states with spin  $|s| > 1$  are stable. Spin-flip processes, however, can induce a relaxation of the total spin. These can be due to different mechanisms such as magnetic scattering and spin-orbit interaction. Another possible source of spin-flip processes can be cotunneling. The quantitative microscopical evaluation of the corresponding relaxation rates is not easy and depends on the dimensionality of the system and on the electronic correlations. In GaAs-based quantum dots, it seems that spin-flip processes have much smaller rates<sup>41</sup>, four orders of magnitude or even smaller than the non-spin-flip processes involved in the relaxation of the bosonic modes. In 1D systems, the non-Fermi liquid nature of the interaction could lead to a non-trivial energy dependence of these relaxation rates.

It is primarily not the aim of the present paper to study these processes. In order to get first insight into the stability of the negative differential conductance features it is sufficient to introduce a *phenomenological* spin-flip relaxation rate  $\Gamma_{s\rightarrow s'}^w$ , with  $s' = s \pm 2$ , and modify accordingly Eq. (31). The results of this modification will be discussed in section VID.

## V. LINEAR TRANSPORT

In this section we specialize (32) to the linear regime ( $V \rightarrow 0$ ). We assume symmetric barriers,  $t_L \equiv t_R$ , and  $C_L \equiv C_R$ , hence we drop for convenience the barrier index in the expression for the rates. The electrochemical potential of the quantum dot is defined as

$$\mu_d(n, s_n) = \mathcal{U}(n+1, s_{n+1}, 0, 0) - \mathcal{U}(n, s_n, 0, 0) \quad (33)$$

where  $s_n, s_{n+1}$  are the spins of the ground state for  $n, n+1$  electrons, respectively. From (9) one finds

$$\mu_d(n, s_n) = E_\rho \left( n + \frac{1}{2} - n_g \right) + (-1)^n \frac{E_\sigma}{2}.$$

In the following, we evaluate the linear differential conductance  $G = \partial I / \partial V|_{V=0}$ .

### A. Low temperature

At low temperatures,  $k_B T \ll E_\sigma$ , the master equation is solved in the subspace defined by the ground states for  $n$  and  $n+1$  electrons. The conductance is

$$G(\xi) = \frac{\beta e^2}{\sqrt{8}} \frac{\Gamma(\xi) e^{-\beta\xi/2}}{\cosh\{\beta\xi + (-1)^n \log 2\}/2} \quad (34)$$

where  $\Gamma(\xi)$  is the rate in (25) and  $\xi = E_\rho [n_g - n_g^{\text{res}}(n, 0)]$  corresponds to the deviation from the resonance peak

position  $n_g^{\text{res}}(n, 0)$  at  $T = 0$ . The latter is determined by the condition  $\mu_d = 0$

$$n_g^{\text{res}}(n, 0) = n + \frac{1}{2} + (-1)^n \frac{E_\sigma}{2E_\rho}. \quad (35)$$

The position of the linear conductance peaks is affected by the spin that leads to an even-odd effect in the distances  $\delta(n \leftrightarrow n+1)$  between conductance peaks

$$\delta(n \leftrightarrow n+1) = 1 + (-1)^{n+1} \frac{E_\sigma}{E_\rho}.$$

This even-odd effect was recently observed in carbon nanotube experiments.<sup>4</sup>

For  $T \neq 0$  the peaks in the conductance no longer occur at the zero temperature positions. Instead, they shift linearly with temperature with slopes that depend on the interaction in the leads (Fig. 5)

$$n_g^{\text{res}}(n, T) = n_g^{\text{res}}(n, 0) + (-1)^{n+1} \phi(g_0) \frac{k_B T}{E_\rho}. \quad (36)$$

Here,  $\phi$  is obtained from the implicit relation

$$\text{Im} \left[ \psi \left( \frac{1}{2g} + i \frac{\phi(g_0)}{2\pi} \right) \right] + \frac{\pi}{2} \tanh \left[ \frac{\log 2 + \phi(g_0)}{2} \right] = 0 \quad (37)$$

with  $\psi(z)$  the digamma-function. Without interaction in the leads ( $g_0 = 1$ ) one recovers the well know result  $\phi(1) = \log 2/2$ .<sup>44</sup>

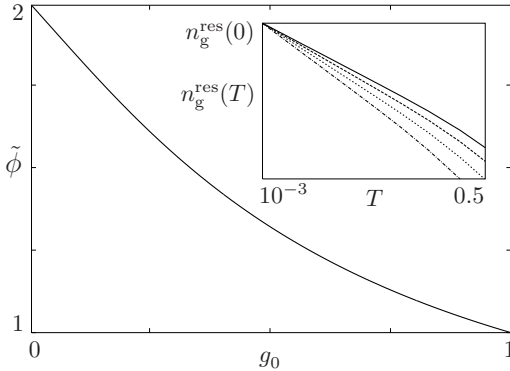


FIG. 5: The prefactor  $\tilde{\phi} = 2\phi(g_0)/\log 2$  in (36) as a function of the interaction in the leads. Inset: low-temperature shift of a conductance peak for  $g_0 = 1.0$  (solid),  $g_0 = 0.8$  (dashed),  $g_0 = 0.6$  (dotted),  $g_0 = 0.4$  (dash-dotted) (temperature units  $E_\sigma/k_B$ ).

For  $k_B T \ll \varepsilon_\nu$ , since one cannot excite charge and spin density waves in the dot, the temperature dependence of the conductance maximum is determined only by the interactions in the leads

$$G^{\text{max}}(T) \propto T^{\alpha-1} \quad (38)$$

with  $\alpha$  given in (27).

## B. High temperature

For  $E_\sigma, \varepsilon_\sigma < k_B T$  the peak position deviates from the linear behavior and approaches, for  $k_B T \approx E_\sigma$ , the spinless value  $n + 1/2$  (Fig. 6). For  $k_B T \gg E_\sigma$ , one obtains

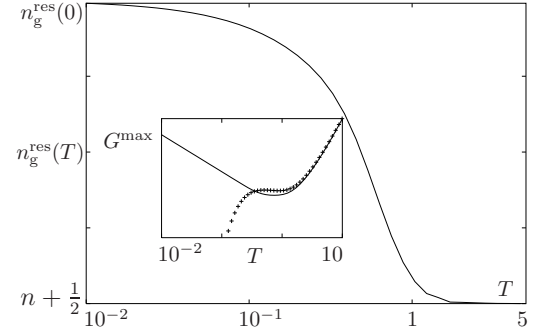


FIG. 6: Position of the conductance peak for even  $n$ , as a function of the temperature  $T$  (units  $E_\sigma/k_B$ ) for  $g_0 = 0.8$ ,  $g_\rho = 0.3$  and  $g_\sigma = 1.0$ . At high temperatures the peak position approaches the spinless value  $n + 1/2$ . Inset: double logarithmic plot of the conductance maximum  $G^{\text{max}}(T)$  in arbitrary units. Crosses: analytic result from (40).

an analytic expression for the conductance. We factorize the occupation probability,  $P_{n,s} = p(n)\Psi(s)$  with  $\Psi(s)$  the thermal occupation probability

$$\Psi(s) = \begin{cases} Z_e^{-1} e^{-\beta E_\sigma s^2/2} & s \text{ even} \\ Z_o^{-1} e^{-\beta E_\sigma (s^2-1)/2} & s \text{ odd} \end{cases} \quad (39)$$

The prefactors  $Z_e = Z_o = \sqrt{\pi/2\beta E_\sigma}$  are determined by the normalization conditions  $\sum_s \Psi(2s) = \sum_s \Psi(2s+1) = 1$ . Using the factorized form for  $P_{n,s}$  we sum over the spin states in the master equation obtaining  $p(n)\tilde{\Gamma}_{n \rightarrow n+1} = p(n+1)\tilde{\Gamma}_{n+1 \rightarrow n}$  ( $n$  even) with

$$\tilde{\Gamma}_{n \rightarrow n+1} = \sum_{p=\pm 1} \int ds e^{-2\beta E_\sigma s^2} \Gamma_{|n, 2s\rangle \rightarrow |n+1, 2s+p\rangle},$$

and

$$\tilde{\Gamma}_{n+1 \rightarrow n} = \sum_{p=\pm 1} \int ds e^{-2\beta E_\sigma (s^2+ps)} \Gamma_{|n+1, 2s+p\rangle \rightarrow |n, 2s\rangle}.$$

The final result for the differential conductance is

$$G(\zeta) = \frac{\beta e^2}{2} \frac{\Gamma(\zeta + E_\sigma/2) \Gamma(-\zeta - E_\sigma/2)}{\Gamma(\zeta + E_\sigma/2) + \Gamma(-\zeta - E_\sigma/2)}, \quad (40)$$

with  $\zeta = E_\rho (n - n_g + 1/2)$ . When  $k_B T \gg E_\sigma$  the conductance peak as extracted from (40) is centered around  $\zeta = 0$  which implies  $n_g^{\text{res}}(n, T) = n + 1/2$ , the spinless position. The conductance peak maximum however follows different power laws depending on the temperature range considered

$$G^{\text{max}}(T) \propto \begin{cases} T^{\alpha-1+(2g_\sigma)^{-1}} & \varepsilon_\sigma \ll k_B T < \varepsilon_\rho \\ T^{\alpha-1+(2g_\sigma)^{-1}+(2g_\rho)^{-1}} & \varepsilon_\rho \ll k_B T < E_\rho \end{cases}$$

Thus, for a well developed energetic separation between charge and spin it should be in principle possible to detect three different power laws in the linear conductance peak maximum value, over the whole temperature range.

## VI. NONLINEAR TRANSPORT

In the following, we discuss the transport in the non-linear regime. We assume  $n$  to be even, then we la-

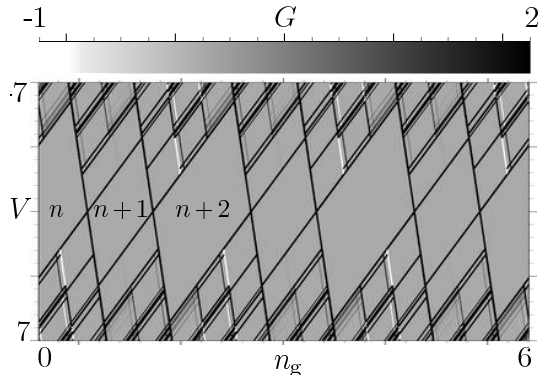


FIG. 7: The differential conductance  $G$  (arbitrary units) as a function of bias voltage  $V$  (units  $E_\sigma/e$ ) and number of gate charges  $n_g$ . System parameters are  $A = G_L/G_R = 50$ ,  $k_B T = 10^{-2} E_\sigma$ ,  $C_L = 5C_R$ ,  $C_g/C_R = 0.01$ ,  $g_\rho = 0.63$ ,  $g_\sigma = 1.15$ ,  $g_0 = 1$ ,  $E_\rho = 5E_\sigma$ . Top: gray scale.

bel the states  $|n, s\rangle$  using the spin variable  $s$  alone such  $\Gamma_{|n,s\rangle \rightarrow |n',s'\rangle}^{(\lambda)} \rightarrow \Gamma_{s \rightarrow s'}^{(\lambda)}$ . The master equation for the stationary probabilities  $P_{n,s}$  is solved numerically. From this the current-voltage characteristic  $I(V, n_g)$  and the differential conductance  $G(V, n_g) = \partial I / \partial V$  are calculated. Figure 7 gives an overview of the behavior of the differential conductance as a function of bias voltage  $V$  and gate voltage induced number of charges  $n_g$ . Most pronounced are the parity effect for  $V \rightarrow 0$  and the rich structure due to the excited states of the quantum dot. This can be understood in detail by considering all the possible transitions and taking into account the correlation induced features of the tunneling rates. Most important are the negative differential conductance peaks indicated by the white lines. They are closely related to the non-Fermi liquid properties of the model. This is discussed below in more detail.

### A. Symmetric barriers

Figure 8 shows the differential conductance  $G(V, n_g)$  for symmetric barriers as a function of bias and gate voltages. The conductance is always positive. Each of the lines corresponds to a peak in the differential conductance and is related to a transition between states in the dot for  $n$  and  $n+1$ .

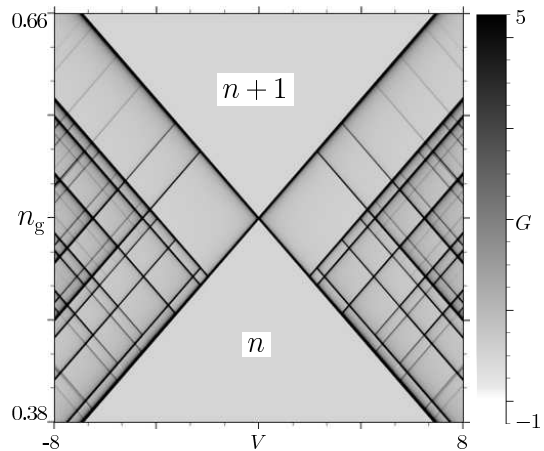


FIG. 8: The differential conductance  $G$  (arbitrary units) as a function of the bias voltage (units  $E_\sigma/e$ ) and  $n_g$ , for symmetric barriers ( $A = 1$ ,  $\eta = 1/2$ ) for  $k_B T = 10^{-2} E_\sigma$ ,  $E_\rho = 25E_\sigma$ ,  $g_0 = 0.9$ ,  $g_\rho = 0.8$ ,  $g_\sigma = 1.15$  corresponding to  $\varepsilon_\sigma/\varepsilon_0 = 0.99$ ,  $\varepsilon_\rho/\varepsilon_0 = 1.42$  and  $2E_\sigma/\varepsilon_0 = 0.86$ . Right: gray scale.

The condition for opening the transition  $|n, s\rangle \leftrightarrow |n+1, s \pm 1\rangle$ , without involving CDW and SDW, is

$$-\eta eV \leq -E_\rho \tilde{n}_g \pm E_\sigma s \leq (1 - \eta)eV. \quad (41)$$

with  $\tilde{n}_g = n_g - n_g^{\text{res}}(n, 0)$  and

$$\eta = \frac{C_R + C_g/2}{C_L + C_R + C_g}.$$

For symmetric barriers  $\eta = 1/2$  and  $A = G_L/G_R = 1$ . The scheme of the transitions consistent with (41) is shown in Fig. 9. States with spin  $s$  and  $-s$  are degenerate (cf. (9)). First, we consider transitions between the ground states,  $|n, 0\rangle \leftrightarrow |n+1, 1\rangle$  associated with the lines  $E_\rho \tilde{n}_g = (\eta - 1)eV$  and  $E_\rho \tilde{n}_g = \eta eV$ , respectively. These lines divide the plane ( $V > 0, n_g$ ) in three regions. The shaded regions labeled  $n$  and  $n+1$  denote the Coulomb blockade regimes with zero conductance. In the other regions, both of the ground states have finite occupation probabilities and the quantum dot is conducting.

Since the state  $|n+1, 1\rangle$  is now occupied, the transition  $|n+1, 1\rangle \rightarrow |n, 2\rangle$  becomes available at sufficiently high voltages. The corresponding activation threshold is given by  $E_\rho \tilde{n}_g = \eta eV - 2E_\sigma$  (cf. (41) with  $s = 2$ ). The transition channel  $|n, 2\rangle \rightarrow |n+1, 1\rangle$  is always open in the transport domain. Inside the domain where  $|n, 2\rangle$  is occupied we can achieve the transition for  $|n, 2\rangle \rightarrow |n+1, 3\rangle$  by increasing  $V$ . By iterating the procedure with increasingly higher values of the spin we get the fish-bone pattern shown in Fig. 9.

So far we only have considered the excited states with higher spin of the dot. In order to complete the picture, we must include all the transitions involving collective charge and spin excitations. This enhances considerably the complexity of the spectrum, since at high enough

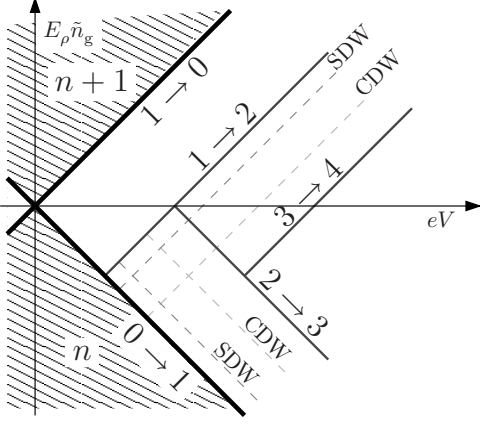


FIG. 9: Scheme of transition lines in the differential conductance for symmetric barriers ( $\eta = 1/2$ ,  $A = 1$ ). Shaded regions denote Coulomb blockade. Thick black lines: ground-state to ground-state transitions; dark-gray sequence of lines: transitions to higher-spin states (spin values of the states involved in the transition are indicated); dashed lines: SDW and CDW excited states. For simplicity we have dropped indices  $n$ ,  $n+1$  denoting the transitions by spin values  $s$  only.

bias voltage each transition of the type  $|n, s\rangle \rightarrow |n', s'\rangle$  can also occur via the channels  $|n, s\rangle \rightarrow |n', s', l_\rho, l_\sigma\rangle \rightleftharpoons |n', s'\rangle$ . For example, consider the CDW- and SDW-channels for the transition  $|n, 0\rangle \rightarrow |n+1, 1\rangle$ . These correspond to the equations  $E_\rho \tilde{n}_g = (\eta - 1)eV + l_\rho \varepsilon_\rho + l_\sigma \varepsilon_\sigma$ . The lines are parallel to the line  $|n, 0\rangle \rightarrow |n+1, 1\rangle$ . Analogously, including CDW- and SDW-channels in the transition  $|n+1, 1\rangle \rightarrow |n, 0\rangle$  gives rise to  $E_\rho \tilde{n}_g = \eta eV + l_\rho \varepsilon_\rho + l_\sigma \varepsilon_\sigma$  and to transition lines parallel to the line  $|n+1, 1\rangle \rightarrow |n, 0\rangle$  (Fig. 9).

### B. Non symmetric barriers

Figure 10 shows the differential conductance for asymmetry  $A = 50$ .

The main difference between the results in Fig. 10 and those obtained for symmetric barriers (cf. Fig. 8) are the negative conductance features associated with the white transition lines. They are due to the presence of interaction,  $\varepsilon_\rho \neq \varepsilon_\sigma$ , as can be seen from Fig. 11 where the differential conductance is shown for  $g_\rho = g_\sigma = 1$ .

For  $V > 0$  electrons flow from right to left. Then, for  $A > 1$  the electrons traverse a higher barrier tunneling into the dot, and a lower barrier tunneling out of the dot. Thus, states  $|n, s\rangle$  will have a higher occupation probability as compared to states  $|n+1, s+1\rangle$ . This “trapping” phenomenon at sufficiently large asymmetries can create a bottleneck for the electron transport and enhances the probability to have a NDC. The occupation probabilities for the lower spin states are shown in Fig. 12 for increasing bias voltage. If the occupation of a higher-spin state e.g.  $(n, 2)$  is favored on the expense of the ground

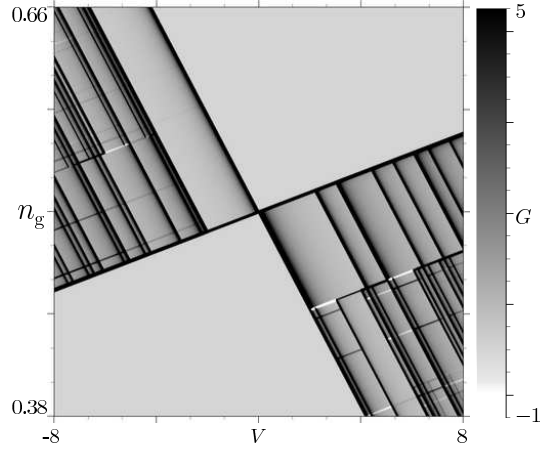


FIG. 10: The differential conductance  $G$  (arbitrary units) as a function of  $V$  (units  $E_\sigma/e$ ) and  $n_g$  for asymmetric barriers with  $A = 50$ ,  $C_L = 5C_R$ ,  $C_g/C_R = 0.01$ ,  $k_B T = 10^{-2} E_\sigma$ ,  $E_\rho = 25E_\sigma$ ,  $g_0 = 0.9$ ,  $g_\rho = 0.8$ ,  $g_\sigma = 1.1$  corresponding to  $\varepsilon_\sigma/\varepsilon_0 = 0.995$ ,  $\varepsilon_\rho/\varepsilon_0 = 1.37$ ,  $2E_\sigma/\varepsilon_0 = 0.9$ . Several transitions associated with NDC (white lines) parallel to transition lines  $|n+1, 2s-1\rangle \rightarrow |n, 2s, \rho, \sigma\rangle$  are observed. Right: gray scale.

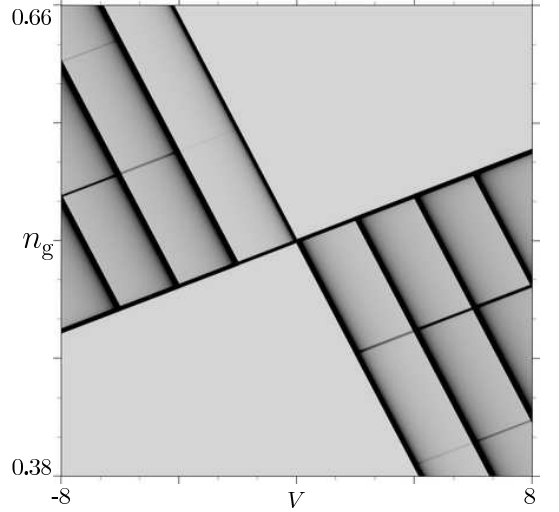


FIG. 11: The differential conductance  $G$  (arbitrary units) as a function of  $V$  (units  $E_\sigma/e$ ) and  $n_g$  for  $A = 50$ ,  $C_L/C_R = 5$ ,  $C_g/C_R = 0.01$ ,  $k_B T = 10^{-2} E_\sigma$ ,  $E_\rho = 25E_\sigma$ ,  $g_0 = 0.9$ ,  $g_\rho = g_\sigma = 1.0$ ,  $2E_\sigma = \varepsilon_\sigma = \varepsilon_\rho = \varepsilon_0$ . Despite the strong asymmetry there is no NDC. Lines parallel to the transitions  $|n+1, 1\rangle \rightarrow |n, 0\rangle$  tend to have very small intensity. Gray scale as in Fig. 10.

state,  $(n, 0)$ , it accumulates occupation probability and this eventually leads to a reduction of the current.

However, it is important to note that trapping alone is not sufficient to induce NDC. If the system does not exhibit spin-charge separation (Fig. 11) no NDC occurs, independent of the strength of the asymmetry. To un-

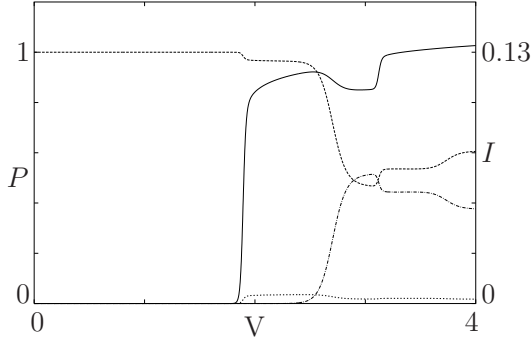


FIG. 12: Occupation probabilities  $P_{n,0}$  (dashed),  $P_{n,2} + P_{n,-2}$  (dashed-dotted),  $P_{n+1,1} + P_{n+1,-1}$  (dotted), and current  $I$  (full line, units  $e\Gamma_0^{(R)}$ ) as a function of the bias voltage  $V$  (units  $E_\sigma/e$ ) for  $n_g = 0.457$ ; other parameters as in Fig. 10.

derstand this point better, we use a simple model that can be treated analytically. We assume  $g_\rho = g_\sigma = g_0 = 1$  and  $k_B T \ll \varepsilon_\sigma$ .

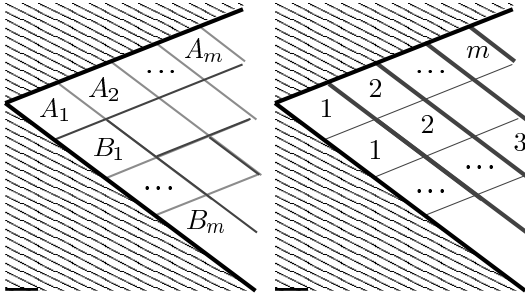


FIG. 13: Transport without spin-charge separation. Left: transition lines for asymmetric barriers ( $A > 1$ ) and  $g_\rho = g_\sigma = 1$ . Right: values for the current  $I$  in units  $I_0 = e\Gamma_0^{(R)}$  for  $A \rightarrow \infty$  and  $T = 0$ , keeping  $G_R$  finite.

We refer to Fig. 13 (left) where several regions of given higher-spin states are shown:  $\{A_m\}$  with  $s_{\max} = 1$ ,  $\{B_m\}$  with  $s_{\max} = 2$ . In these regions the transition rates occur in a well defined pattern. For instance, for  $\{A_m\}$  we have  $\Gamma_{0 \rightarrow 1}^{(R)} = m\Gamma_0^{(R)}$  and  $\Gamma_{1 \rightarrow 0}^{(L)} = \Gamma_0^{(L)}$ , while for  $\{B_m\}$  we have  $\Gamma_{0 \rightarrow 1}^{(R)} = \Gamma_0^{(R)}$ ,  $\Gamma_{1 \rightarrow 0}^{(L)} = (m+1)\Gamma_0^{(L)}$ ,  $\Gamma_{1 \rightarrow 2}^{(L)} = m\Gamma_0^{(L)}$  and  $\Gamma_{2 \rightarrow 1}^{(R)} = 2\Gamma_0^{(R)}$ . This allows to solve the master equation and evaluate the currents (cf. Fig. 13 right) for  $A \rightarrow \infty$ . This limit is performed by assuming  $G_R$  finite and corresponds to the most favorable situation for generating NDC. One finds that the conductance lines parallel to  $|n+1, 1\rangle \rightarrow |n, 0\rangle$  vanish. The lines parallel to  $|n, 0\rangle \rightarrow |n+1, 1\rangle$  correspond to PDC. Thus, for  $A \rightarrow \infty$ , the absence of charge-spin separation leads to a landscape of PDC peaks. The numerical results for  $A = 50$  (Fig. 11) are consistent with this picture. We have confirmed numerically that the above results remain valid also for interacting leads,  $g_0 < 1$ , and for  $T \neq 0$ .

### C. The five-states model

Among the transitions in Fig. 10 which show NDC, we will concentrate on those in the gray region for the transition  $|n, 2\rangle \rightarrow |n+1, 1\rangle$  (cf. Fig. 14). This is divided into three regions I, II, III depending on the presence of SDW and CDW states,  $l_\sigma = l_\rho = 0$ ;  $l_\sigma = 1, l_\rho = 0$ ;  $l_\sigma = 0, l_\rho = 1$ , respectively. Here, only the five states  $|n, 0\rangle$ ,  $|n+1, \pm 1\rangle$ ,  $|n, \pm 2\rangle$  contribute to transport. For

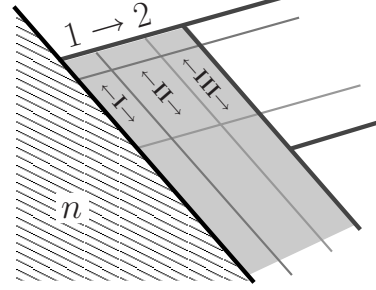


FIG. 14: Regions analyzed analytically with respect to the NDC: I, II, III correspond to  $l_\sigma = l_\rho = 0$ ;  $l_\sigma = 1, l_\rho = 0$ ;  $l_\sigma = 0, l_\rho = 1$ , respectively, in the transition  $|n, 2\rangle \rightarrow |n+1, 1\rangle$ .

these, the master equation is solved analytically. The current is

$$I = e \frac{2\Gamma_{0 \rightarrow 1}^{(R)} \left[ \Gamma_{1 \rightarrow 0}^{(L)} + \Gamma_{1 \rightarrow 2}^{(L)} \right] \Gamma_{2 \rightarrow 1}^{(R)}}{\Gamma_{1 \rightarrow 0}^{(L)} \Gamma_{2 \rightarrow 1}^{(R)} + 2\Gamma_{0 \rightarrow 1}^{(R)} \left[ \Gamma_{2 \rightarrow 1}^{(R)} + \Gamma_{1 \rightarrow 2}^{(L)} \right]}, \quad (42)$$

with the transition energies  $\Delta U_{0 \rightarrow 1} = eV - 2E_\sigma$ ,  $\Delta U_{2 \rightarrow 1} = eV$ ,  $\Delta U_{1 \rightarrow 0} = 2E_\sigma$  and  $\Delta U_{1 \rightarrow 2} = 0$  inside the corresponding rates. For  $k_B T \ll E_\sigma$  and  $g_0$  not too small, one can assume that along the lines  $|n+1, 1\rangle \rightarrow |n, 2\rangle$ ,  $|n+1, 1\rangle \rightarrow |n, 0, 0, 1\rangle$ ,  $|n+1, 1\rangle \rightarrow |n, 0, 1, 0\rangle$ , and not too close to the crossing points, the only rates that contribute to the derivative with respect to  $V$  are  $\Gamma_{1 \rightarrow 2}^{(L)}$  and  $\Gamma_{1 \rightarrow 0}^{(L)}$ . With this the differential conductance is

$$G = \frac{e\phi_0}{\mathcal{D}_0^2} \sum_{p=\pm 1} \Lambda_p \partial_V \Gamma_{1 \rightarrow 1+p}^{(L)}(V), \quad (43)$$

where  $\phi_0 = 2\Gamma_{0 \rightarrow 1}^{(R)} \Gamma_{2 \rightarrow 1}^{(R)}$  and

$$\begin{aligned} \Lambda_p &= \phi_0 + p \left( \Gamma_{2 \rightarrow 1}^{(R)} - 2\Gamma_{0 \rightarrow 1}^{(R)} \right) \Gamma_{1 \rightarrow 1-p}^{(L)} \\ \mathcal{D}_0 &= \Gamma_{1 \rightarrow 0}^{(L)} \Gamma_{2 \rightarrow 1}^{(R)} + 2\Gamma_{0 \rightarrow 1}^{(R)} \left( \Gamma_{2 \rightarrow 1}^{(R)} + \Gamma_{1 \rightarrow 2}^{(L)} \right). \end{aligned} \quad (44)$$

Expression (43) can change sign depending on the factor  $\Lambda_p$ . For  $G$  along  $|n+1, 1\rangle \rightarrow |n, 2, l_\rho, l_\sigma\rangle$  we have  $p = 1$ , and  $p = -1$  for  $G$  along  $|n+1, 1\rangle \rightarrow |n, 0, l_\rho, l_\sigma\rangle$ . Consider the transition  $|n+1, 1\rangle \rightarrow |n, 2\rangle$ , thus  $p = +1$ . Along this line,  $\Gamma_{2 \rightarrow 1}^{(R)}$  has contributions from the excited states, while the other rates are  $\Gamma_0^{(L, R)}$ . For non-

interacting leads,  $g_0 = 1$ , the condition  $\Lambda_1 \leq 0$  is equivalent to

$$\left[ \frac{\Gamma_0^{(R)}}{\Gamma_{2 \rightarrow 1}^{(R)}} - \frac{1}{2} \right] A \geq 1.$$

We define  $A_c$  as the critical asymmetry above which NDC is found. In region I,  $A_c^{(I)} = 2$ . In region II,  $A_c^{(II)} = 2(2g_\rho + 1)/(2g_\sigma - 1) > A_c^{(I)}$ . Thus, for  $A > A_c^{(II)}$  one has NDC in both regions I and II. On the other hand, the condition for having NDC in region III is

$$\frac{A}{2} \left( \frac{2g_\rho g_\sigma - g_\rho - g_\sigma}{2g_\rho g_\sigma + g_\rho + g_\sigma} \right) \geq 1. \quad (45)$$

For small exchange interactions this requirement cannot be fulfilled. Indeed for  $V_{\text{ex}} \leq V_0/2$  one has  $g_\sigma^2 + 3g_\rho^2 - 4g_\rho^2 g_\sigma^2 > 0$  which cannot be satisfied simultaneously with (45). We conclude that for sufficiently large asymmetry NDC is generally found in regions I and II and PDC in region III at the transition  $|n+1, 1\rangle \rightarrow |n, 2\rangle$ .

The conditions for NDC along the lines  $|n+1, 1\rangle \rightarrow |n, 0, 0, 1\rangle$  and  $|n+1, 1\rangle \rightarrow |n, 0, 1, 0\rangle$  is

$$\left[ \frac{1}{2} - \frac{\Gamma_0^{(R)}}{\Gamma_{2 \rightarrow 1}^{(R)}} \right] A \geq 1.$$

It is clear that both in I and in II no NDC are found. In zone III, however, it is possible to have  $\Gamma_{2 \rightarrow 1}^{(R)} > 2\Gamma_0^{(R)}$  with NDC for

$$A > A_c^{(III)} = 2 \frac{g_\rho + g_\sigma + 2g_\rho g_\sigma}{g_\rho + g_\sigma - 2g_\rho g_\sigma}$$

If  $A > \max\{A_c^{(I)}, A_c^{(II)}, A_c^{(III)}\}$  the NDC-PDC pattern has therefore a "photographic-negative"-like shape. This means that if the line  $|n+1, 1\rangle \rightarrow |n, 2\rangle$  ( $p = +1$ ) has NDC, the two adjacent ones ( $p = -1$ ) have PDC, and *vice versa*. This feature can be found in many regions of the density plot for not too high bias voltage (cf. Fig. 7).

These results indicate that in addition to the condition  $\varepsilon_\rho \neq \varepsilon_\sigma$  one must have non-integer steps in the transition rates as a function of the energy in order to find NDC. It seems that this is a genuine feature in present case of an interacting system with non-Fermi liquid correlations, i.e. with spin-charge separation.

#### D. Spin-flip relaxation

Since the NDC is related to the occupation of states with spins higher than that of the ground state, it is of great interest to introduce into the master equation an extra spin-flip relaxation rate  $\Gamma_{s \rightarrow s'}^w$ . This will give insight into the depletion behavior of the NDC when spin-flip processes are present. We assume

$$\Gamma_{s \rightarrow s'}^w = \begin{cases} w & |s'| < |s| \\ w \exp[-\frac{1}{2}\beta E_\sigma (s'^2 - s^2)] & |s'| > |s| \end{cases}, \quad (46)$$

with  $s' = s \pm 2$ ,  $n' = n$ , and consider  $w$  to be an estimate of the typical spin-flip rate. This spin-flip mechanism acts against the trapping of the higher spin states, providing an escape possibility  $|n, 2\rangle \rightarrow |n, 0\rangle$ . This is expected to decrease the chance to have NDC.

The differential conductance for different values of the spin relaxation rate  $w$  is shown in Fig. 15 for voltages within the five-states region,  $s_{\text{max}} = \pm 2$ . The peaks for a positive bias are reduced by increasing  $w$ , especially the NDC state which eventually becomes positive. For negative bias, electrons traverse a lower barrier tunneling into the dot, and a higher barrier tunneling outside:  $P_{n,0}, P_{n,\pm 2} < P_{n+1,\pm 1}$ . Therefore the relaxation from the states  $|n, \pm 2\rangle$  is almost influential, since these states have already a small occupation probability.

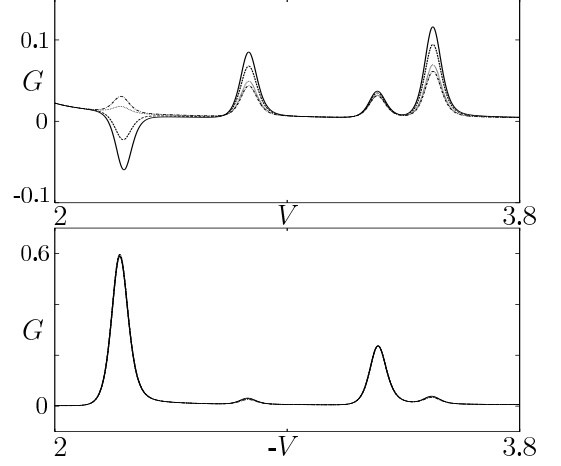


FIG. 15: Differential conductance (units  $e^2\Gamma_0^{(R)}/E_\sigma$ ) a function of positive and negative voltages  $V$  (units  $E_\sigma/e$ ) in the five-states region for  $n_g = 0.485$  for spin relaxation rates  $w = 0.2$  (solid), 0.3 (dashed), 0.5 (dotted) and 0.6 (dash-dotted) in units  $\Gamma_0^{(L)}(E_\sigma/\omega_c)^\alpha$ , for  $k_B T = 10^{-2}E_\sigma$ ,  $E_\rho = 25E_\sigma$ ,  $A = 10$ ,  $\eta = 1/2$ ,  $g_0 = 0.9$ ,  $g_\rho = 0.7$  and  $g_\sigma = 1.25$ .

As an example, we consider the above five-states model including spin-flip relaxation. The conductance has the same form as in (43)

$$G = \frac{e\phi_w}{\mathcal{D}_w^2} \sum_{p=\pm 1} \Lambda_p^w \partial_V \Gamma_{1 \rightarrow 1+p}^{(L)}(V) \quad (47)$$

but now  $\phi_w = 2\Gamma_{0 \rightarrow 1}^{(R)}(w + \Gamma_{2 \rightarrow 1}^{(R)})$  and

$$\begin{aligned} \Lambda_p^w &= \phi_w + p \left[ \Gamma_{2 \rightarrow 1}^{(R)} - 2\Gamma_{0 \rightarrow 1}^{(R)} \right] \Gamma_{1 \rightarrow 1-p}^{(L)} \\ \mathcal{D}_w &= \Gamma_{1 \rightarrow 0}^{(L)} \Gamma_{2 \rightarrow 1}^{(R)} + 2\Gamma_{0 \rightarrow 1}^{(R)} \left[ \Gamma_{2 \rightarrow 1}^{(R)} + \Gamma_{1 \rightarrow 2}^{(L)} \right] \\ &\quad + w \left[ \Gamma_{1 \rightarrow 0}^{(L)} + \Gamma_{1 \rightarrow 2}^{(L)} + 2\Gamma_{0 \rightarrow 1}^{(R)} \right]. \end{aligned} \quad (48)$$

As above, the sign of the conductance is solely given by  $\Lambda_p^w$  which is now a function both of the asymmetry and of the relaxation  $w$ . We concentrate on the region I ( $2E_\sigma <$

$eV < \varepsilon_\sigma$ ) of the line  $|n+1, 1\rangle \rightarrow |n, 2\rangle$ . The condition  $\Lambda_1^w \leq 0$  reduces at  $T = 0$  to

$$\frac{w}{\Gamma_0^{(L)}} \leq \left(\frac{2E_\sigma}{\omega_c}\right)^\alpha \left[1 - \frac{1}{2} \left(\frac{eV}{eV - 2E_\sigma}\right)^\alpha - \frac{1}{A} \left(\frac{eV}{2E_\sigma}\right)^\alpha\right]$$

with  $\alpha$  given in (27). The critical value  $w_c$  for the

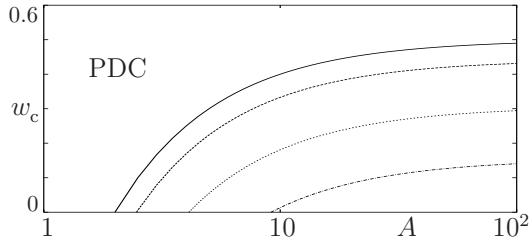


FIG. 16: Phase diagram for the critical value of the spin-flip relaxation rate  $w$  (units  $\Gamma_0^{(L)}(E_\sigma/\omega_c)^\alpha$ ) in region I as a function of the asymmetry  $A$  for  $T = 0$  and different interaction parameters in the leads:  $g_0 = 1.0$  (solid),  $g_0 = 0.9$  (dashed),  $g_0 = 0.75$  (dotted) and  $g_0 = 0.65$  (dash-dotted).

crossover is plotted in Fig. 16 as a function of  $A$ . At a given asymmetry, for  $w > w_c$  the conductance peak crosses over to positive values. The stronger the interaction in the leads the smaller is the threshold in the relaxation for destroying the NDC peak.

## VII. CONCLUSIONS

We have investigated the non-linear current voltage characteristic of a 1D quantum dot described by a Luttinger liquid of a finite length connected via tunnel barriers to interacting quantum wires. The system contains four characteristic energy scales: charge and spin addition energies, and the energies needed to excite charge and spin density collective modes in the quantum dot. We have discussed in particular the effects related to the presence of the electron spin.

In the linear regime, we have reproduced the parity effect in the distances between the Coulomb blockade conductance peaks. In contrast to the case without interaction discussed earlier,<sup>44</sup> the temperature behavior of the peak positions shows signatures of the non-Fermi liquid nature of the leads. At temperatures higher than the spin addition energy, the peaks become equidistant.

In non-linear transport, we have found NDC features that are related to the presence of spin-charge separation. They are connected to states with higher spins that participate in the electron transport.

This effect is different from the spin blockade phenomenon discussed previously.<sup>7</sup> In the spin blockade of type I, a “trapping” argument is used to explain the effect. However, in this case the only state that leads to trapping (and thus can decrease the current) is a state

with the highest total spin and highest energy for a given electron number. Thus, only one NDC peak can be present in a given  $n \leftrightarrow n+1$  transition. The “trapped” status is achieved because of the Clebsch-Gordan coefficients that are introduced in the calculation of the transition rates.

In contrast, in the present case, each state with even (odd) spin can become trapped if  $(A-1)V > 0$  ( $< 0$ ) such that the transition lines that populate such a state exhibit NDC. Whether or not such a state is eventually trapped is determined by the transition rates which are here microscopically evaluated using the Luttinger liquid model. The result is that even if the system contains asymmetric barriers that lead to trapping of the appropriate candidate states in the dot, it is still necessary to have charge-spin separation in order to obtain NDC. It is clear from the above that the effect of spin-charge separation is not only the trivial removal of energetic degeneracy of the CDW and SDW states. The spectral weights contained in the tunneling rates (25) play a crucial role in determining whether or not a particular transition line corresponds to NDC.

Since NDC is driven by asymmetry, there must be a threshold value  $A_c$  above which the phenomenon occurs. This critical value is not universal. Each transition line has a different critical value for the asymmetry.

We have assumed that the collective excitations that do not alter the  $z$ -component of the spin in the quantum dot have infinitely short relaxation times as compared with the excitations which are associated with spin changes. We feel that this assumption is justified in view of recent results suggesting that in quantum dots the relaxation of states without flipping spins can be orders of magnitudes shorter than that associated with spin flips.<sup>41</sup> Nevertheless, the question whether or not without this assumption the predicted NDC-phenomena would disappear is legitimate. In order to answer this question quantitatively, it is necessary to repeat the calculations including the collective states of the quantum dot as dynamical variables in the master equation.<sup>40</sup>

Spin-flip relaxation processes only seem to weaken existing NDCs, as indicated by the results in the section VID. Thus, we can expect that by removing relaxation processes and including additional stable states in the transport process without flipping the total spin will not change qualitatively the trapping mechanism described in the section VIB. The NDC predicted here, which appears to be a consequence of the trapping mechanism and the separation of energy scales for spin and charge excitations together with the Luttinger liquid features that enter the rates, will not be depleted.

In experiment, several possibilities for measuring the predicted non-linear phenomena exist. The necessary condition for applying the above model is

$$k_B T \ll \varepsilon_0 \ll E_F, \quad (49)$$

with  $\varepsilon_0 = \pi v_F/a$ . This is equivalent to

$$\lambda_T \gg a \gg \lambda_F \quad (50)$$

where  $\lambda_T = \pi v_F/k_B T$  is the thermal length and  $\lambda_F = 2\pi/k_F$  the Fermi wave length. Tunnel barriers will in general be asymmetric in any case.

In semiconductor based quantum wires, quantum dots are prepared via depleting the electron density such that eventually an electronic island is formed accidentally between two impurities.<sup>20</sup> In this system, the Fermi energy appears to be relatively low,  $E_F \approx 2$  meV, due to the almost depletion of the lowest sub-band.<sup>21</sup> The dot energy level spacing is about 1 meV for a quantum dot of length  $a \approx 0.2 \mu\text{m}$  and an effective mass  $m^* \approx 0.07 m_e$  (for GaAs). These parameters at the first glance seem to be outside the above region of validity of the model, although the condition with respect to the temperature is easily fulfilled. For a quantum dot of larger size ( $a \approx 1 \mu\text{m}$ ) the situation would be much more favorable. This seems to be achievable in other semiconductor based quantum dot systems, such as those fabricated by scratching techniques.<sup>45</sup> With this one could fabricate an appropriately scaled quantum dot in a quantum wire. Parameters to be achieved should be: width of wire  $\approx 50$  nm in order to make a Fermi energy of a few meV achievable; distance between the tunnel barriers (point contacts) that define the quantum dot  $\approx 1 \mu\text{m}$  giving  $\varepsilon_0 \approx 0.1$  meV. Temperatures should be well below 1K.

With this technique, one would have the advantage of being able to adjust the asymmetry of the tunnel barriers.

In carbon nanotubes the situation with respect to the energy scales seems to be even more favorable since  $E_F \approx 2$  eV,  $v_F \approx 8 \cdot 10^5$  m/s and the level spacing  $\varepsilon_0 \approx 5$  meV with temperatures of the order  $T \approx 100$  mK.<sup>4</sup> However, here the non-interacting energy spectrum consists of four branches including the spin. The present theory has to be adjusted to this case in order to apply the results. Again, due to the fact that the predicted phenomenon seems to be quite generally valid, one can expect that experiments on carbon nanotubes should show NDC associated with the higher spin states.

### Acknowledgments

We are grateful for helpful and illuminating discussions with Rolf Haug. Financial support by the European Union via TMR-networks FMRX-CT98-0180 and HPRN-CT2000-0144, and from the Italian MURST PRIN02 is gratefully acknowledged.

- 
- <sup>1</sup> G. A. Prinz, Phys. Today **48**, 58 (1995); Science **282**, 1660 (1998).
- <sup>2</sup> J. M. Kikkawa, and D. D. Awschalom, Phys. Rev. Lett. **80**, 4313 (1998); D. D. Awschalom, and J. M. Kikkawa, Phys. Today **52**, 33 (1999).
- <sup>3</sup> S. Tarucha, D. G. Austing, T. Honda, R. J. van der Hage, and L.P. Kouwenhoven, Phys. Rev. Lett. **77**, 3613 (1996).
- <sup>4</sup> D. H. Cobden, M. Bockrath, P. L. McEuen, A. G. Rinzler, and R. E. Smalley, Phys. Rev. Lett. **81**, 681 (1998); D.H. Cobden, and J. Nygård, Phys. Rev. Lett. **89**, 046803 (2002).
- <sup>5</sup> M.R. Buitelaar, A. Bachtold, T. Nussbaumer, M. Iqbal, and C. Schönberger, Phys. Rev. Lett. **88**, 156801 (2002).
- <sup>6</sup> D. Weinmann, W. Häusler, W. Pfaff, B. Kramer, and U. Weiss, Europhys. Lett. **26**, 467 (1994).
- <sup>7</sup> D. Weinmann, W. Häusler, and B. Kramer, Phys. Rev. Lett. **74**, 984 (1995).
- <sup>8</sup> M. Ciorga, A. Wensauer, M. Pioro-Ladriere, M. Korkusinski, J. Kyriakidis, A. S. Sachrajda, and P. Hawrylak, Phys. Rev. Lett. **88**, 256804 (2002).
- <sup>9</sup> K. Jauregui, W. Häusler, D. Weinmann, and B. Kramer, Phys. Rev. B **53**, R1713 (1996).
- <sup>10</sup> A. K. Huettel, H. Qin, A. W. Holleitner, R. H. Blick, K. Neumaier, D. Weinmann, K. Eberl, and J. P. Kotthaus, Europhys. Lett. **62**, 712 (2003).
- <sup>11</sup> S. Tarucha, T. Honda, and T. Saku, Sol. St. Commun. **94**, 413 (1995).
- <sup>12</sup> A. Yacoby, H. L. Stormer, N. S. Wingreen, L. N. Pfeiffer, K. W. Baldwin, and K. W. West, Phys. Rev. Lett. **77**, 4612 (1996).
- <sup>13</sup> A. Yacoby, H. L. Stormer, K. W. Baldwin, L. N. Pfeiffer, and K. W. West, Solid State Commun. **101**, 77 (1997).
- <sup>14</sup> O. M. Auslaender, A. Yacoby, R. de Picciotto, K. W. Baldwin, L. N. Pfeiffer, and K. W. West, Science **295**, 825 (2002).
- <sup>15</sup> Y. Tserkovnyak, B. I. Halperin, O. M. Auslaender, and A. Yacoby, Phys. Rev. Lett. **89**, 136805 (2002); Phys. Rev. B **68**, 125312 (2003).
- <sup>16</sup> H.W.Ch. Postma, M. de Jonge, Z. Yao, and C. Dekker, Phys. Rev. B **62**, R10653 (2000).
- <sup>17</sup> W. Liang, M. Bockrath, and H. Park, Phys. Rev. Lett. **88**, 126801 (2002).
- <sup>18</sup> Yu. V. Nazarov, and L. I. Glazman, Phys. Rev. Lett. **91**, 126804 (2003).
- <sup>19</sup> D. G. Polyakov, and I. V. Gornyi, Phys. Rev. B **68**, 035421 (2003).
- <sup>20</sup> O.M. Auslaender, A. Yacoby, R. de Picciotto, K.W. Baldwin, L.N. Pfeiffer, and K.W. West, Phys. Rev. Lett. **84**, 1764 (2000).
- <sup>21</sup> T. Kleimann, M. Sassetti, B. Kramer, and A. Yacoby, Phys. Rev. B **62**, 8144 (2000).
- <sup>22</sup> A. Braggio, M. Sassetti, and B. Kramer, Phys. Rev. Lett. **87**, 146802 (2001).
- <sup>23</sup> A. Imamoglu, D. D. Awschalom, G. Burkard, D. P. DiVincenzo, D. Loss, M. Sherwin, and A. Small, Phys. Rev. Lett. **83**, 4204 (1999).
- <sup>24</sup> P. Recher, E. V. Sukhorukov, and D. Loss, Phys. Rev. Lett. **85**, 1962 (2000).
- <sup>25</sup> H. A. Engel, and D. Loss, Phys. Rev. Lett. **86**, 4648 (2001).
- <sup>26</sup> A. Brataas, Y. V. Nazarov, and G.E.W. Bauer, Phys. Rev. Lett. **84**, 2481 (2000).
- <sup>27</sup> Q. Si, Phys. Rev. Lett. **81**, 3191 (1998).
- <sup>28</sup> L. Balents, and R. Egger, Phys. Rev. Lett. **85**, 3464 (2000).
- <sup>29</sup> J. Voit, Rep. Progr. Phys. **58**, 977 (1995).

- <sup>30</sup> S. Tomonaga, *Prog. Theor. Phys.* **5**, 544 (1950).
- <sup>31</sup> J. M. Luttinger, *J. Math. Phys.* **4**, 1154 (1963).
- <sup>32</sup> F. D. M. Haldane, *J. Phys. C* **14**, 2585 (1981).
- <sup>33</sup> I. Safi, and H. J. Schulz, *Phys. Rev. B* **52**, R17040 (1995).
- <sup>34</sup> T. Kleimann, F. Cavaliere, M. Sasseti, and B. Kramer, *Phys. Rev. B* **66**, 165311 (2002).
- <sup>35</sup> M. Fabrizio, and A. O. Gogolin, *Phys. Rev. B* **51**, 17827 (1995).
- <sup>36</sup> A. E. Mattsson, S. Eggert, and H. Johannesson, *Phys. Rev. B* **56**, 15615 (1997).
- <sup>37</sup> M. Sasseti, and B. Kramer, *Phys. Rev. Lett.* **80**, 1485 (1998).
- <sup>38</sup> G.-L. Ingold, and Yu. V. Nazarov in “Single charge tunneling”, ed. by H. Grabert, and M. H. Devoret, NATO ASI series B **294**, p. 21 (1992).
- <sup>39</sup> A. Furusaki, *Phys. Rev. B* **57**, 7141 (1998).
- <sup>40</sup> J. U. Kim, I. V. Krive, and J. M. Kinaret, *Phys. Rev. Lett.* **90**, 176401 (2003).
- <sup>41</sup> A. V. Khaetskii, and Yu. V. Nazarov, *Phys. Rev. B* **61**, 12639 (2000).
- <sup>42</sup> J. U. Kim, J. M. Kinaret, M. -S. Choi, *cond-mat/0403613* (2004).
- <sup>43</sup> A. Braggio, R. Fazio, and M. Sasseti *Phys. Rev. B* **67**, 233308 (2003).
- <sup>44</sup> G. Usaj, and H. U. Baranger, *Phys. Rev. B* **64**, 201319 (2001).
- <sup>45</sup> H. W. Schumacher, U. F. Keyser, U. Zeitler, R. J. Haug, K. Eberl, *Appl. Phys. Lett.* **75**, 1107 (1999).